

Filament attachment dynamics in actin-based propulsion

J. I. Katz*

*Department of Physics and McDonnell Center for the Space Sciences,
Washington University, St. Louis, Mo. 63130*

A. E. Carlsson†

Department of Physics, Washington University, St. Louis, Mo. 63130

(Dated: November 19, 2018)

Abstract

Theory and experiment have established that F-actin filaments are strongly attached to the intracellular parasites (such as *Listeria*) they propel with “comet tails”. We consider the implications of these observations for propulsion. By calculating the motion produced in various models of attachment and comparing to experiment we demonstrate that the attachment must be sliding rather than hinged. By modeling experiments on ActA-coated spheres we draw conclusions regarding the interaction between F-actin and their surfaces that may also be applicable to living systems.

PACS numbers: 87.15.Kg, 87.16.Ac, 87.17.Aa, 87.17.Jj

*Electronic address: katz@wuphys.wustl.edu; Work supported by NIH grant GM38542

†Electronic address: aec@wuphys.wustl.edu; Work supported by NIH grant GM38542

I. INTRODUCTION

A number of intracellular parasites, some of medical as well as scientific interest, propel themselves through host cells by suborning the host's actin polymerization machinery, inducing it to provide propulsive force for the parasite [1, 2, 3, 4, 5, 6, 7, 8, 9, 10, 11]. These parasites include *Listeria monocytogenes*, *Shigella flexneri*, *Rickettsiae* and *Vaccinia* virus. Catalytic proteins on the surface of the parasite initiate the growth of new polymeric (F-) actin filaments on the surface.

F-actin appears to be tightly bound to the surface it pushes. Evidence for binding [12, 13, 14, 15, 16, 17, 18] includes measurement of discrete displacement steps nearly equal to the diameter (5.4 nm) of G-actin, direct observation and the theoretical argument that in the absence of binding Brownian diffusion would readily sever the contact between the parasite and its propelling bundle of F-actin filaments (called a comet-tail, from its micrographic appearance). Angular diffusion is also rapid in the absence of binding; for a sphere of radius $r = 1\text{ }\mu\text{m}$, $D_\theta = kT/8\pi\eta r^3 = 0.16\text{ radian}^2/\text{sec}$, taking the viscosity η of pure water; the effective viscosity of cytoplasm is greater, scale dependent and poorly understood [19, 20, 21]. Even if the effective viscosity were 100 times greater, unattached bacteria would tumble rapidly, in contradiction to observation.

Maintaining contact over a time t requires an attractive potential $V \leq -kT \ln(\nu t)$, where ν is a relaxation rate (an effective attempt frequency). A number of processes contribute to ν : viscous drag on the sphere, the (damped) elastic modes of the actin filaments, and elastic/plastic flow of the actin gel embedded in the surrounding aqueous medium. Of these, only the first is known quantitatively: The viscous damping of a μm -sized object of density ρ and radius r gives $\nu = 9\eta/(2\rho r^2) \sim 10^7\text{ sec}^{-1}$ (in water). Taking $t \geq 10^3\text{ sec}$ as an empirical lower bound on the attachment time we find $V \leq -1.0 \times 10^{-19}\text{ J}$ [15]. Because the dependence of V on ν is logarithmic, this result is only weakly dependent on uncertainties (such as the applicable viscosity) in ν .

The interaction between a filament of F-actin and the protein-covered surface to which it is bound is complex, and not calculable from *ab initio* interatomic potentials. The purpose of this work is to constrain that interaction by calculating the consequences for propulsion of simple models of the interaction, and then comparing the results to experiment.

Intercalation is driven by the free energy [22] $\Delta G \approx 6 \times 10^{-20}\text{ J}$ released when a molecule

of G-actin is added to a filament of F-actin. During intercalation a single filament exerts a force $F \sim \Delta G/a \approx 20$ pN on the G-actin, drawing it into the gap between the F-actin and the surface proteins to which it is bound. This force is sufficient to drive μm -sized objects at speeds ~ 0.1 cm/sec against viscous drag (taking the viscosity to be that of water), so the intercalation is complete and ΔG dissipated in a few μsec . The product of the duration of a single intercalation $t_I = 6\pi\eta a^2 r / \Delta G$ (the force must move the sphere and the filament to make room for the intercalated monomer) and the Brownian relaxation rate ν of a propelled sphere defines a new dimensionless number which we call the intercalation smoothness

$$N_{IS} \equiv t_I \nu = \frac{27\pi\eta^2 a^2}{\Delta G \rho r}. \quad (1)$$

The intercalating Reynolds number of both the sphere and the G-actin are

$$\text{Re} = \frac{9}{2} \frac{a}{r} \frac{1}{N_{IS}} \ll 1. \quad (2)$$

When $N_{IS} \gg 1$ and $\text{Re} \ll 1$, as is the case here ($N_{IS} \approx 10^2$ for $r = 0.25 \mu\text{m}$, taking the viscosity of pure water) the Stokes flow approximation (implicitly averaging over the sphere's and filament's Brownian motion) may be used during the intercalation, even though the entire intercalation is effectively instantaneous compared to the intervals between intercalations. N_{IS} is related to the Reynolds number, but not entirely determined by it because of the additional factor $a/r \sim 10^{-2}$. There are parameter regimes (not relevant to the experiments discussed here) for which both $\text{Re} \ll 1$ and $N_{IS} \ll 1$, so that Stokes flow would be applicable but in which it would not be valid to average over the Brownian motion of the sphere or filament.

II. CALCULATIONS

We have performed Monte-Carlo simulations of the effects of G-actin intercalation in a model in which the F-actin is attached to the surface of a sphere. This model is necessarily much simplified compared to a full physical description. For example, we employ crude approximations to the flow around the sphere with attached F-actin and ignore cross-linking within the actin tail. Recognizing the crudity of our models, we note that doing better would require either formidable numerical calculations (for example, of the flow around a sphere with attached filaments) and quantitative understanding (of actin cross-linking, and

of the precise geometry of the attached filaments) which does not exist. Despite these rough approximations, we believe our qualitative conclusions are reliable and useful.

We use three-dimensional physics except for a model of the geometry in which the F-actin is constrained to lie in a single equatorial disc. We take the flow fields to be those of Stokesian flow around a sphere. The surrounding fluid, as is generally the case in low Reynolds number hydrodynamics [23], is an effectively infinite sink of momentum and angular momentum, just as it is also a heat bath.

The crucial question is the mechanism by which the symmetry of a particle initially uniformly covered with intercalation sites is broken, producing directed motion. Symmetry is much simpler to define and easier to achieve on the rim of a disc (on which equally spaced points are equivalent) than on the surface of a sphere (on which it is not, in general, possible to distribute N equivalent points). Symmetry-breaking results from amplification of statistical fluctuations in the locations of the intercalation sites, which depend on N but not on dimensionality.

At the beginning of a Monte Carlo run N ($N = 50$ in the calculations shown here), intercalation sites are distributed uniformly around the rim of the disc. By eliminating any statistical deviation from symmetry in the location of sites we focus attention of the mechanism by which symmetry is broken. The loci of intercalation events are chosen randomly from these sites. The time scale is arbitrarily defined by an assumed intercalation rate, but all other parameters are physically meaningful. Each intercalation introduces a relative displacement of $a = 2.7$ nm between the F-actin (initially containing zero monomers) and its attachment point. This displacement is divided between the filament and the sphere in inverse proportion to their viscous drags (using the three dimensional results for an isolated sphere without attached filaments and a prolate ellipsoid [23, 24]). Their mutual hydrodynamic interaction and their interactions with the other filaments are small and not calculable analytically, and are ignored. The displacement of the attachment point is resolved into a radial part, which displaces the disc, and a tangential part, which rotates it.

When the disc is displaced it is surrounded by a Stokes flow field (taken to be that of a sphere). All filaments are immersed in this flow field, affect it, and move with it. A quantitative calculation of the flow field would not be feasible in this complex geometry, so we approximate it by assuming each filament, if free to rotate, is rotated about its attachment point by an angle $\Delta\theta = fa \sin \phi / (r + \ell/2)$, where f is the fraction of the relative

displacement accommodated by the disc, ℓ is the length of the filament, $r = 0.25 \mu\text{m}$ is the sphere's radius and ϕ is the angle between the radius vector to the attachment point and the sphere's displacement vector. This approximates moving the midpoint of the (nearly rigid) filament along with its local (Stokesian) flow field around a sphere. If the attachment points are permitted to slide along the sphere's periphery they are displaced by an angle (measured at the center of the equatorial disc) $\Delta\theta = fa \sin \phi / (r + \ell/2)$; a small minimum angular separation between filaments is imposed. We consider only a single particle in an infinite fluid; this amounts to requiring that any walls or other particles or filaments are many times more distant than the diameter of the sphere or the length of the filament.

Similarly, when the sphere is rotated there is a surrounding Stokesian [23] flow field. We approximate the rotation of each filament about its attachment point by an angle $\Delta\theta = (3/4)fa \sin \theta_t / (r + \ell/2)$, where the numerator is the displacement of the disc circumference and θ_t is the initial angle between the filament and the normal at its attachment point.

We first consider a model in which the attachments are fixed hinges. Initially, intercalation produces only infinitesimal displacement of the sphere because as $\ell \rightarrow 0$, $f \rightarrow 0$. As the filaments lengthen $f \rightarrow 1$ and the sphere's displacement at each intercalation increases. The rotation of the filaments around their hinges, resulting from their viscous drag, now leads to their being swept back in a direction opposite to the sphere's motion. Once swept back, further intercalation tends, on average, to propel the sphere in the direction of its earlier motion. The symmetry of the initial conditions is broken by the stochastic fluctuations in the intercalation sites, and the sphere acquires a systematic motion. Increasing orientational asymmetry of the filaments leads to preferential motion in the direction opposite to the mean filament, and further orientation of the filaments in that direction as the process runs away. The Reynolds number remains small, so this is not an inertial effect; the directional memory resides in the orientation of the filaments.

In a second model the attachment points are free to slide along the surface of the sphere as they are swept back by the Stokes flow, but are held perpendicular to the sphere, as is considered, for example, by [17] (and is achieved in simple mechanical devices). No torques are exerted on the sphere so it does not systematically rotate. Once statistical fluctuations break the initial symmetry, intercalation between swept-back filaments and the sphere preferentially pushes the sphere in the direction of its earlier motion. This process then runs away. As before, the Reynolds number remains very small and the directional

memory resides in the locations of the filaments' attachment points.

III. RESULTS

Results of numerical simulation of the hinged model are shown in Fig. 1 and Fig. 2. Initially random fluctuations first give way to directed displacement. Later, rotation runs away as it sweeps the filaments back around their hinges, and this orientation contributes to further rotation like a pinwheel. The mean speed then drops, directed displacement ends, and no comet-tail forms.

Results for the sliding model are shown in Fig. 3 and Fig. 4. The random number generator was initialized with the same seed as in Fig. 1 and Fig. 2; the initial motion is very similar because little rotation or translation of the filaments has occurred in either model. However, between 7500 and 10000 steps (the fourth and fifth “sunbursts” in the upper right panel of Fig. 3) the attachments have slid significantly and directed motion has begun. Soon thereafter, this process runs away, the filaments condense to an ordered comet-tail, and the motion becomes steady and directed. Within the limits of the computational model (which has no surrounding cytoskeleton or branching or cross-linking of filaments), this is a satisfactory representation of the observed comet-tails.

IV. DISCUSSION

These results may help explain the experiments of [25, 26, 27], in which polystyrene spheres partially but spherically symmetrically (as well as can be achieved experimentally) coated with the actin polymerization-stimulating protein AcTa and immersed in cytoplasm (*Xenopus* egg extract) were observed after a latency time to break their initial symmetry and develop comet-tails of F-actin and directed motion. This behavior is similar to that which we find with sliding attachments (as pointed out in [16], in this experiment the ActA may “crawl” on the surface of the beads).

The most remarkable feature of these experiments is the non-monotonic dependence of bead motility (and comet-tail formation) on the fraction of bead surface covered by ActA, peaking around 3/8 coverage. This is naturally explained by our calculations, for a bead sparsely covered with ActA will develop little propulsive force (bead motion is restrained

by pre-existing cytoskeleton), while a bead completely covered offers no room for the ActA, and attached F-actin, to be swept back into a comet-tail. Thus, from these experiments and our calculations we determine the properties of the F-actin binding to the bead surface and constrain microscopic mechanical models such as those of [17]. In contrast, experiments [28] in which ActA is covalently bound to beads do not show comet tails and propulsion, which is attributable to the inability of covalently bound ActA to slide over the beads' surfaces.

Latency was also found in experiments [29] on spheres in a synthetic growth medium. In these experiments beads continuously covered with actin did move, but in a saltatory manner, apparently as a result of elastic stresses [30] (not considered here) in a fractured continuous shell of F-actin. When the coverage was only partial, the motion was continuous, resembling the results of [25] and agreeing with our calculations.

Acknowledgments

We thank S. Block, J. Cooper, A. Mogilner, D. Sept and J. Theriot for useful discussions.

-
- [1] S. Cudmore *et al.*, Nature (London) **378**, 636 (1995).
 - [2] J. A. Theriot, Ann. Rev. Cell Dev. Biol. **11**, 213 (1995).
 - [3] S. Dramsi and P. Cossart, Ann. Rev. Cell Dev. Biol. **14**, 137 (1998).
 - [4] F. Gerbal, *et al.*, Pramana **53**, 155 (1999).
 - [5] R. A. Heinzen, *et al.*, Infect. Immun. **67**, 4201 (1999).
 - [6] D. Bray, Genome Biology **1**, 108.1 (2000)
 - [7] G. G. Borisy and T. M. Svitkina, Current Opinion in Cell Biol. **12**, 104 (2000).
 - [8] L. A. Cameron *et al.*, Nature Rev. Mol. Cell Biol. **1**, 110 (2000).
 - [9] L. A. Cameron *et al.*, Current Biol. **11**, 130 (2001).
 - [10] J. A. Theriot, Traffic **1**, 19 (2000).
 - [11] D. Pantaloni, C. LeClainche and M.-F. Carlier, Science **292**, 1502 (2001).
 - [12] S. C. Kuo and J. L. McGrath, Nature (London) **407**, 1026 (2000).
 - [13] F. Gerbal, *et al.*, Biophys. J. **79**, 2259 (2000).
 - [14] F. Gerbal, *et al.*, Euro. Biophys. J. **29**, 134 (2000).

- [15] D. J. Olbris and J. Herzfeld, *Biochem. Biophys. Acta* **1495**, 140 (2000).
- [16] A. D. Rutenberg and M. Grant, *Phys. Rev. E* **64**, 021904 (2001).
- [17] R. B. Dickinson and D. L. Purich, *Biophys. J.* **82**, 605 (2002).
- [18] A. Mogilner and G. Oster, *Biophys. J.* **84**, 1591 (2003).
- [19] J. L. McGrath, *et al.*, *Biophys. J.* **75**, 2070 (1998).
- [20] A. R. Bausch, W. Möller and E. Sackmann, *Biophys. J.* **76**, 573 (1999).
- [21] K. Luby-Phelps, *Int. Rev. Cytology* **192**, 189 (2000).
- [22] D. J. Gordon, Y.-Z. Yang and E. D. Korn, *J. Biol. Chem.* **251**, 7474 (1976).
- [23] J. Happel and H. Brenner, *Low Reynolds Number Hydrodynamics* (Kluwer, Boston, 1983).
- [24] H. C. Berg, *Random Walks in Biology* (Princeton U. Press, Princeton, 1983) p. 57.
- [25] L. A. Cameron *et al.*, *PNAS* **96**, 4908 (1999)
- [26] A. van Oodenaarden and J. A. Theriot, *Nature Cell Biol.* **1**, 493 (1999).
- [27] L. A. Cameron, *et al.*, *Mol. Biol. Cell* **15**, 2312 (2004).
- [28] V. Noireaux *et al.*, *Biophys. J.* **78**, 1643 (2000).
- [29] A. Bernheim-Groswasser *et al.*, *Nature (London)* **417**, 308 (2002).
- [30] K. Sekimoto, *et al.*, *Eur. Phys. J. E* **13**, 247 (2004).

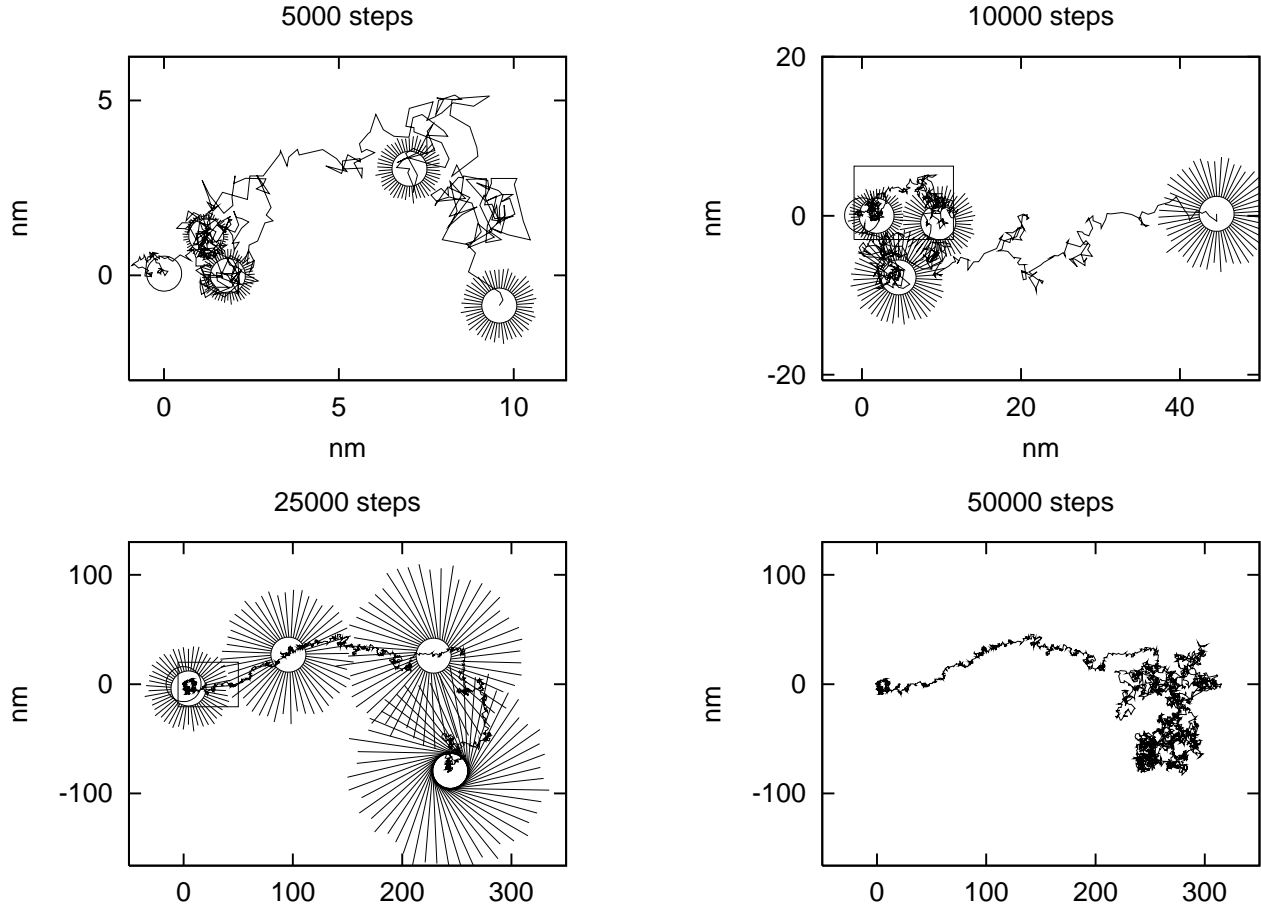


FIG. 1: The motion of a representative sphere with hinged attachments. The “sunbursts” show the sphere and attached filaments (the relative dimensions of sphere and filaments are correct, but not on the same scale as the paths). The rectangles in some frames show the sizes of the previous frames for comparison. An initial random walk soon yields to directed motion, but around step 20000 runaway “pinwheel” rotation becomes dominant. The rotation at the hinges is evident in the sunburst for step 25000. The last frame shows the end of directed motion.

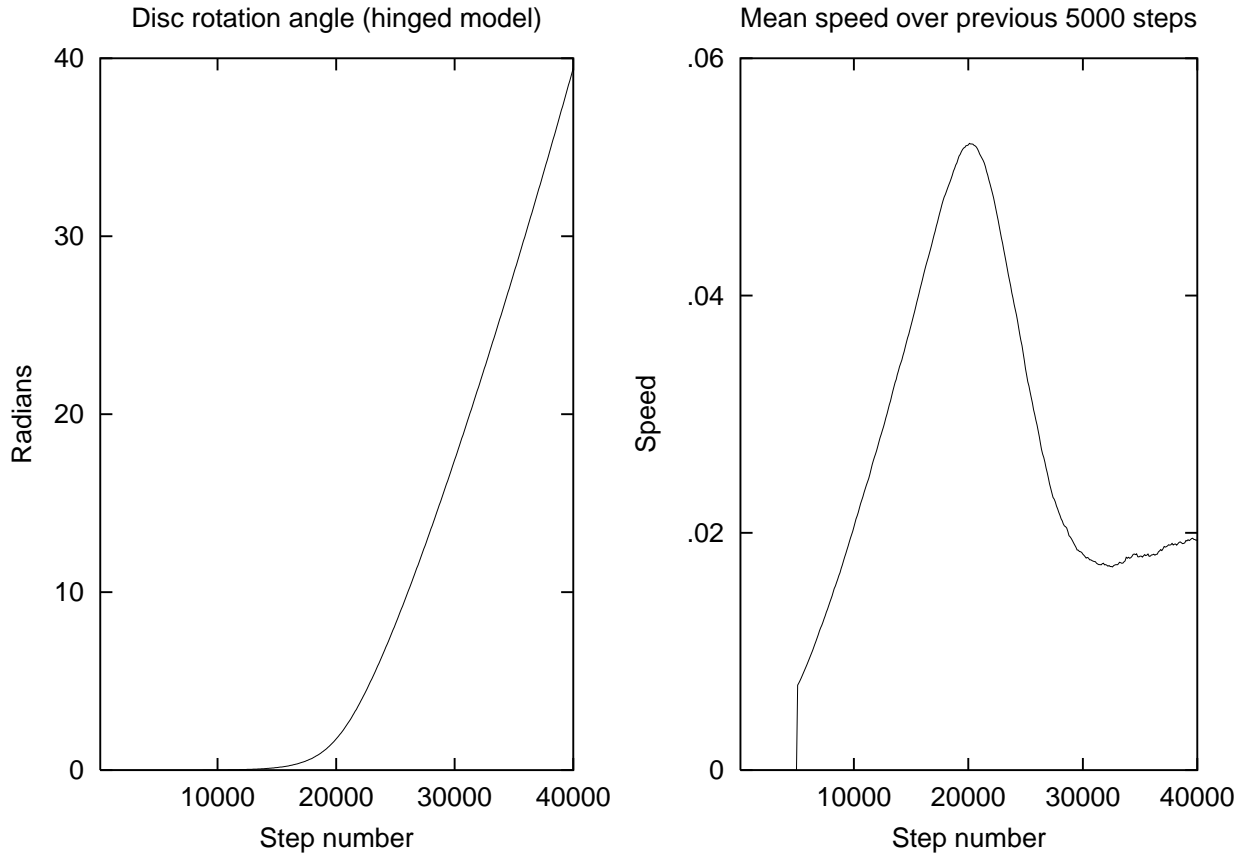


FIG. 2: Averages (over 1000 runs) of the absolute value of the disc rotation angle and mean speed (arbitrary units) for hinged attachments. Runaway “pinwheel” rotation beginning around step 20000 is evident, with a corresponding decrease in mean speed. The mean filament length is the step number divided by the number of filaments, 50 in this calculation.

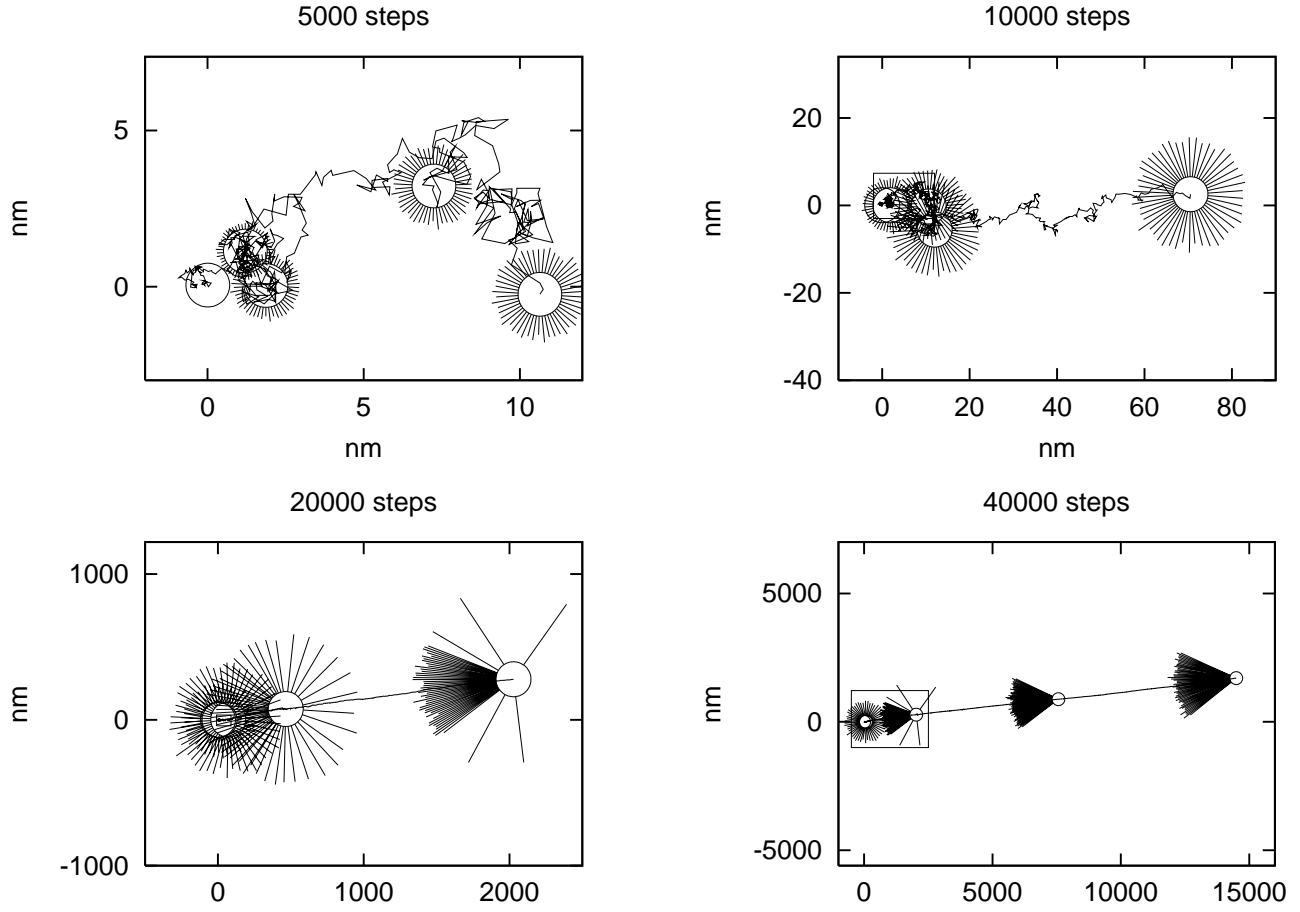


FIG. 3: The motion of a representative disc with sliding normal attachment. “Sunbursts” and rectangles are as in Fig. 1. Initially random motion gives way to directed motion and the formation of a comet-tail. An arbitrary minimum angle between filaments prevents the collapse of the comet tail to a single line.

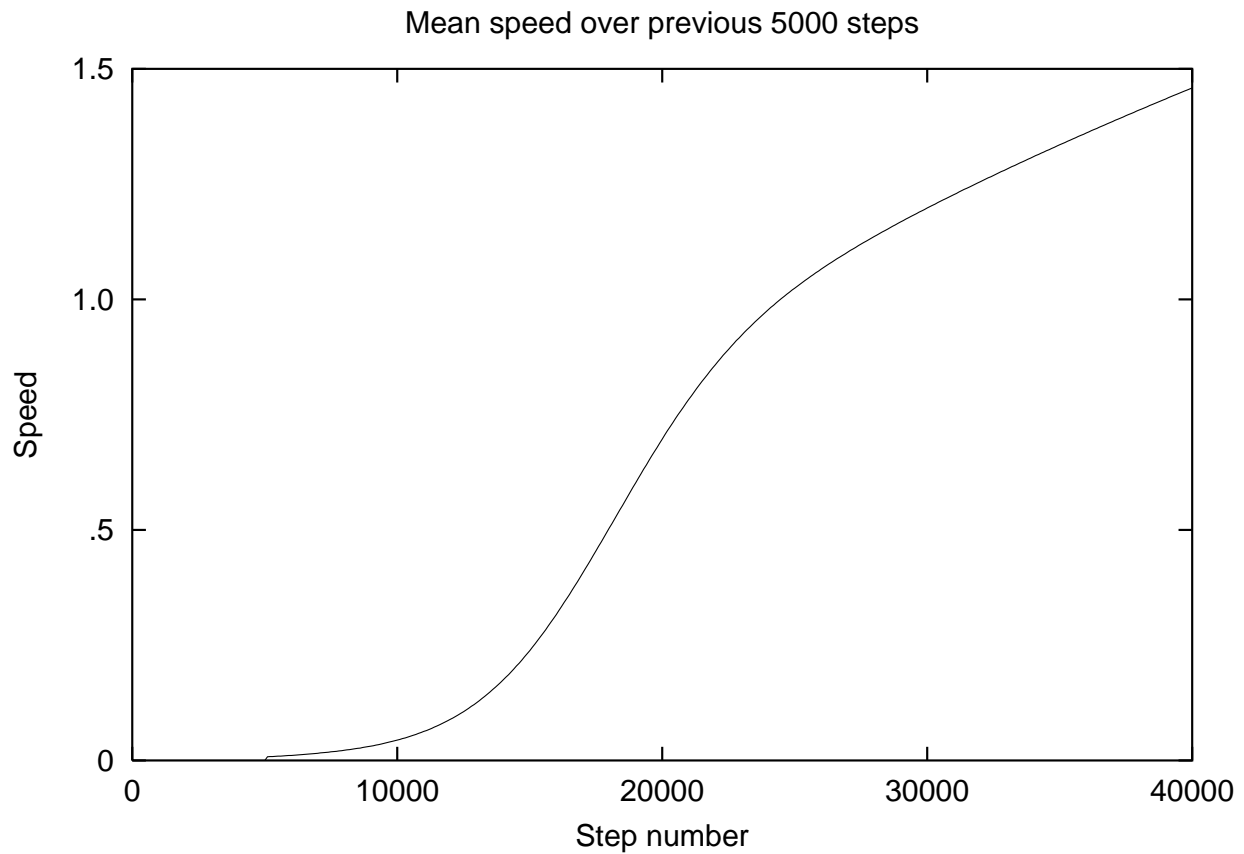


FIG. 4: Average (over 1000 runs) of the mean disc speed with sliding attachments, showing acceleration as the filaments are swept back into a coherent comet-tail. The speed is in the same units as, and should be compared to, Fig. 2; it continues to increase $\propto f \rightarrow 1$ after a comet tail is formed around step 20000.